ASEAN Journal of Science and Engineering

Journal homepage: http://ejournal.upi.edu/index.php/AJSE/

Compressive Performance and Predictive Modelling of Recycled Brick Aggregate Concrete Confined with Basalt Fiber-Reinforced Polymer for Supporting Sustainable Development Goals (SDGs)

Phromphat Thansirichaisree[1], Ali Ejaz[2], Hisham Mohamad[3], Preeda Chaimahawan[4], Qudeer Hussain[5]*

[1]Thammasat University, Klong Luang, Pathumthani, Thailand,
[2]National University of Sciences and Technology, Islamabad, Pakistan
[3]Universiti Teknologi PETRONAS, Seri Iskandar, Malaysia
[4]University of Phayao, Phayao, Thailand
[5]Kasem Bundit University, Thailand
[*]Correspondence: E-mail: preeda.ch@up.ac.th

ABSTRACT

This study aimed to investigate the antimicrobial potential of four imidazolium-based salt derivatives (A1–A4) using an integrated approach that combined in vitro biological assays with computational analysis. The compounds were screened against various Gram-positive and Gram-negative bacteria, as well as fungal strains, while computational methods like ADMET predictions and molecular simulations assessed their viability and mechanism. The results revealed that compounds A3 and A4 possess potent antibacterial activity comparable to gentamicin, particularly against *E. coli*, with A3 also showing significant antifungal efficacy. These findings were strongly supported by computational analysis, which predicted favorable oral bioavailability, acceptable toxicity, and confirmed a stable binding interaction with the bacterial enzyme DNA gyrase. The primary implication is the identification of A3 and A4 as promising therapeutic candidates for developing new antimicrobials to combat drug-resistant pathogens, validating this integrated research strategy for future drug discovery.

ARTICLE INFO

Article History:
Submitted/Received 27 May 2025
First Revised 28 Jun 2025
Accepted 30 Aug 2025
First Available online 31 Aug 2025
Publication Date 01 Mar 2026

Keyword:
Basalt FRP,
Design-oriented model,
Nonlinear regression,
Recycled brick aggregates,
Compressive strength,
Ultimate strain.

1. INTRODUCTION

The demolition of aging structural units has led to a substantial global accumulation of construction waste. China alone, for instance, generates an estimated 1.8 billion tons of demolition waste annually, reflecting the scale of the challenge in managing such material effectively and the growing scarcity of natural aggregates used in construction [1-3]. Repurposing demolition debris offers a practical solution, as it helps reduce construction waste, conserves natural resources, and lowers disposal costs [4-7]. Accordingly, the search for sustainable, cost-efficient, and environmentally friendly alternatives has intensified, and several studies have highlighted the viability of using construction and demolition waste as partial substitutes for natural aggregates [8-13].

Recycled aggregates from demolition waste are typically categorized into recycled concrete aggregates (sourced entirely from processed concrete) and mixed recycled aggregates, which include bricks, concrete, and tiles [14]. Recycled concrete aggregates constitute approximately 40% of the total supply, while mixed recycled aggregates account for the remaining 60% [14]. Regulations in many countries permit the partial replacement of natural aggregates with recycled concrete aggregates, usually within a range of 20% to 30% . Numerous studies confirm that such replacement levels can yield concrete with acceptable mechanical performance [15, 16].

In recent years, fired clay bricks have been reused as coarse aggregate replacements in concrete mixes [17]. Experimental studies demonstrated that aggregates derived from fired-clay bricks can produce concrete with satisfactory strength characteristics [18]. However, other findings indicate that concrete containing recycled bricks typically exhibits lower density and compressive strength compared to natural aggregate concrete (NAC) [19]. For example, the use of different brick types has been shown to result in reductions in compressive and flexural strengths relative to NAC [20]. Additional research supports the feasibility of brick aggregate use, while also highlighting its generally reduced strength and stiffness [21-23].

The compressive strength and ductility of concrete can be enhanced through lateral confinement, employing methods such as stirrups, steel jackets, or fiber-reinforced polymer (FRP) wraps [24-27]. Among these, synthetic FRP sheets (especially carbon, glass, and aramid-based types) have been widely used due to their high in-plane stiffness [28-33]. Hybrid FRPs have also been explored for improved performance [34]. Nonetheless, high costs and the potential health risks associated with the chemical constituents in synthetic FRPs remain key limitations [35-38]. Alternative confinement strategies, such as large rupture strain FRPs, have also been proposed for structural retrofitting applications [39-41].

Basalt fiber-reinforced polymer (BFRP) has emerged as a promising alternative due to its cost-effectiveness and favorable mechanical and chemical properties [42]. Basalt fibers, produced through the high-temperature extrusion of volcanic rock, retain most of their mechanical strength even after prolonged thermal exposure, and their manufacturing process is both eco-friendly and additive-free [43]. Compared with carbon FRPs, basalt fibers are considerably more affordable and offer superior modulus and impact resistance relative to glass fibers [44-46]. Furthermore, BFRP typically provides greater ductility than CFRP, making it particularly attractive for structural applications [47, 48]. Prior studies confirm the efficacy of BFRP in strengthening concrete beams, columns, and reinforced concrete frames [46, 49, 50]. Additionally, research has explored the compressive performance of BFRP-confined concrete and the development of confinement models applicable to such systems [51, 52].

DOI: https://doi.org/10.17509/ajse.v6i1.89929
p- ISSN 2776-6098 e- ISSN 2776-5938

Building upon these findings, the present study investigates the structural potential of BFRP in confining recycled brick aggregate concrete (ReBAC), using two types of bricks commonly found in Thailand: fired-clay solid and fired-clay hollow bricks. To the best of the authors' knowledge, no existing research has examined the role of BFRP in enhancing the compressive performance of ReBAC. Therefore, this study aims to (i) evaluate the effectiveness of BFRP confinement in improving the compressive behavior of ReBAC, (ii) assess the accuracy of existing analytical models for predicting compressive strength and strain, and (iii) develop new predictive expressions for strength, strain, and stress–strain response of BFRP-confined ReBAC. The findings are expected to contribute to the advancement of sustainable construction practices by integrating waste-derived aggregates with natural fiber-based confinement, in line with the objectives of the Sustainable Development Goals (SDGs).

2. METHODS

2.1. Details of Specimens

This study employed an experimental program comprising 48 cylindrical specimens, divided into two main groups (**Table 1**). A typical workflow chart is shown in **Figure 1 (a)**. The grouping was based on the type of recycled aggregates, namely fired-clay solid (FCS) bricks and fired-clay hollow (FCH) bricks. Each group consisted of 24 specimens, further subdivided into three subgroups according to unconfined compressive strength levels: low, medium, and high. Each subgroup included four specimens. One specimen served as a reference and was tested in an unstrengthened condition, while the other three were strengthened with two, four, or six layers of BFRP. Two samples were cast for each specimen type, resulting in a total of 48 specimens. A four-part nomenclature was adopted to designate each specimen. The first part, "Cy," indicated the cylindrical specimen; the second part denoted the unconfined strength level (low, medium, or high); the third part represented the type of brick aggregate (FCS for fired-clay solid and FCH for fired-clay hollow); and the fourth part specified the number of BFRP layers. A typical cylindrical specimen is illustrated in **Figure 1 (b)**.

Table 1. Details and grouping of cylinders.

Group	Subgroup	Name	Aggregate Type	Layer
1	I	Cy-L-FCS-Con	Fired-clay solid	None
		Cy-L-FCS-2BFRP		2
		Cy-L-FCS-4BFRP		4
		Cy-L-FCS-6BFRP		6
	II	Cy-M-FCS-Con		None
		Cy-M-FCS-2BFRP		2
		Cy-M-FCS-4BFRP		4
		Cy-M-FCS-6BFRP		6
	III	Cy-H-FCS-Con		None
		Cy-H-FCS-2BFRP		2
		Cy-H-FCS-4BFRP		4
		Cy-H-FCS-6BFRP		6
2	IV	Cy-L-FCH-Con	Fired-clay hollow	None
		Cy-L-FCH-2BFRP		2
		Cy-L-FCH-4BFRP		4
		Cy-L-FCH-6BFRP		6

DOI: https://doi.org/10.17509/ajse.v6i1.89929
p- ISSN 2775-6793 e- ISSN 2775-6815

Table 1 (Continue). Details and grouping of cylinders.

Group	Subgroup	Name	Aggregate Type	Layer
2	V	Cy-M-FCH-Con	Fired-clay hollow	None
		Cy-M-FCH-2BFRP		2
		Cy-M-FCH-4BFRP		4
		Cy-M-FCH-6BFRP		6
	VI	Cy-H-FCH-Con		None
		Cy-H-FCH-2BFRP		2
		Cy-H-FCH-4BFRP		4
		C-HS-CBB-6BFRP		6

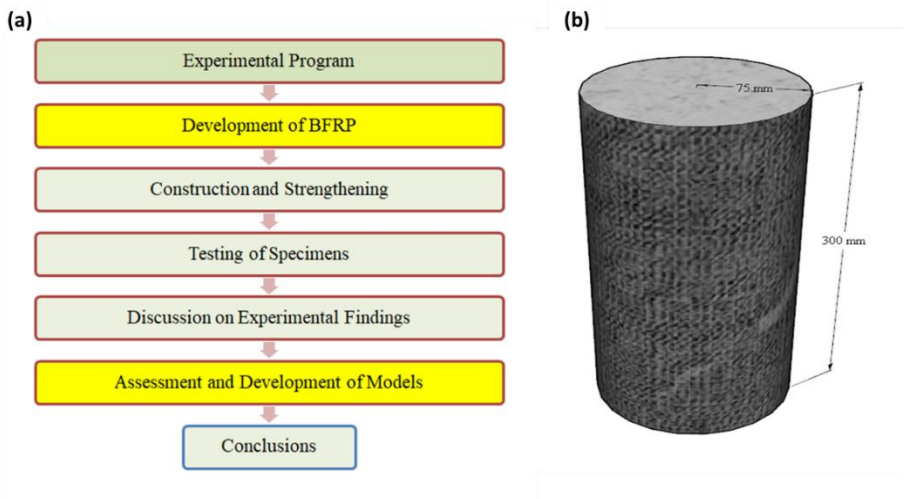

Figure 1. (a) Typical schematic of research, and (b) Typical specimen geometry.

2.2. Material Properties

The properties of recycled bricks were determined in accordance with ASTM C1314-23a, and the results are summarized in **Table 2**. The bricks were crushed using a crusher machine, with the maximum recycled aggregate size limited to 19 mm. Natural river sand was employed as fine aggregate, while Type I Portland cement was used as the binder.The target slump values corresponding to low, medium, and high-strength mixes were 12, 9, and 7 cm, respectively. The detailed concrete mix proportions for each strength level are presented in **Table 3**.

Table 2. Details and grouping of cylinders.

Mechanical Properties	Solid Clay Brick	Hollow Clay Brick
Density (kg/m3)	120	140
Compressive Strength (MPa)	3.14	8.10
Water Absorption (%)	23.2	16.5

Table 3. Concrete mix proportions.

Mix constituents (kg/m3)	Low Strength (15 MPa)	Medium Strength (25 MPa)	High Strength (35 MPa)
Cement	242	343	444
Fine aggregates	726	670	605
Natural coarse aggregates	605	500	504
Clay brick aggregates	605	500	504

DOI: https://doi.org/10.17509/ajse.v6i1.89929
p- ISSN 2776-6098 e- ISSN 2776-5938

In this study, BFRP composites were fabricated using unidirectional natural basalt fabric in combination with polyester resin. The material properties of the BFRP were evaluated in accordance with ASTM D7565/D7565M-10, which outlines procedures for determining the tensile properties of fiber-reinforced polymer composites used for structural strengthening. Following this standard, five tensile specimens were tested using a universal testing machine under a constant loading rate of 5 N/min. The tested BFRP exhibited a thickness of 0.19 mm, a tensile strength of 240 MPa, and an ultimate fracture strain of 2.6%. The typical appearance of the BFRP sheet used in this study is shown in **Figure 2(a),** while the crushed recycled aggregates obtained from fired-clay solid bricks and fired-clay hollow bricks are illustrated in **Figures 2(b)** and **2(c)**, respectively.

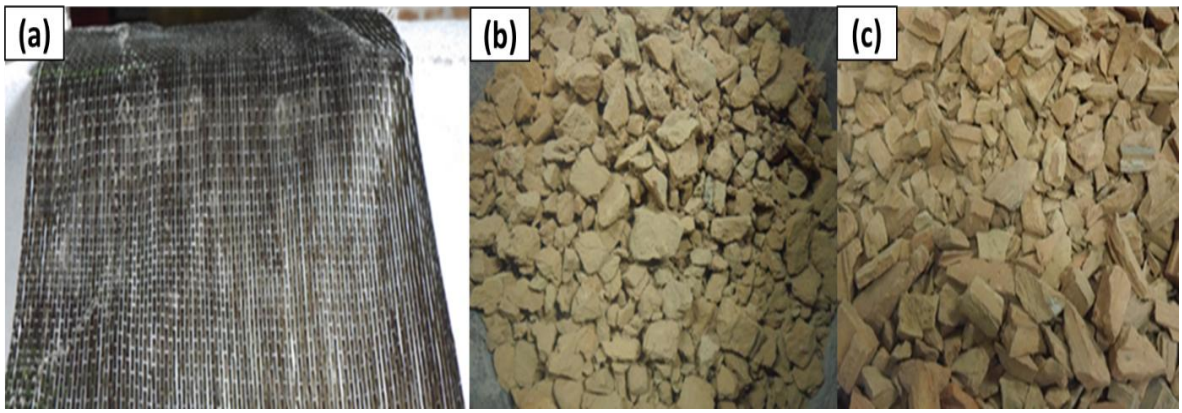

Figure 2. (a) Typical BFRP used in this work, (b) recycled aggregates from fired clay solid bricks, and (c) recycled aggregates from fired clay hollow bricks.

2.3. Construction of specimens

The specimen preparation followed a typical construction procedure. The concrete ingredients were mixed in a mechanical mixer, and the fresh concrete was placed into steel molds in three equal layers, with proper compaction applied to each layer.

After 24 hours, the cylinders were demolded and subjected to a 27-day curing period. For strengthening, the wet lay-up method was employed to apply the BFRP layers. The surface of the cured concrete was first impregnated using an epoxy-saturated roller.

A BFRP sheet was then wrapped around the specimen. For subsequent layers, additional epoxy was applied over the previously bonded BFRP surface to ensure a strong interfacial bond between layers.

2.4. Experimental Setup

A universal testing machine (UTM) with a capacity of 1000 kN was used to apply monotonically increasing compressive loads to the specimens. The applied load was measured using a load cell and continuously recorded by a data logger.

Axial deformation (reduction in specimen height) was monitored using displacement transducers. The compressive strain was then calculated by dividing the measured axial deformation by the original specimen height. A typical test configuration is illustrated in **Figure 3**.

DOI: https://doi.org/10.17509/ajse.v6i1.89929
p- ISSN 2775-6793 e- ISSN 2775-6815

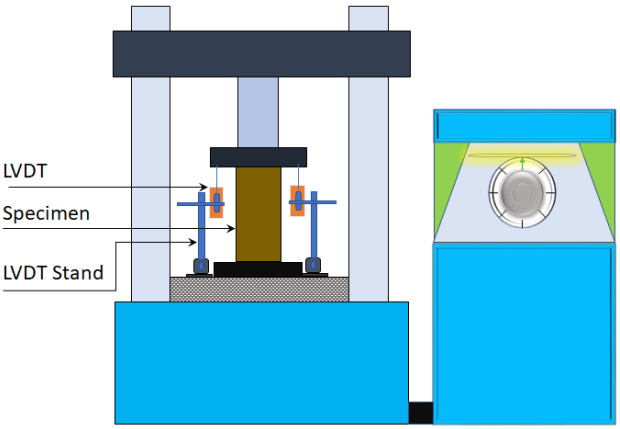

Figure 3. Test setup adopted.

3. RESULTS AND DISCUSSION

3.1. Failure Patterns

The failure patterns of Group 1 and Group 2 cylinders are presented in **Figures 4** and **5**, respectively. All specimens exhibited compressive-type failures, which could generally be classified into three stages: crack initiation, crack propagation, and ultimate failure. Notably, no visible cracks were observed before the specimens reached their peak compressive strength. With further loading, short vertical cracks began to appear, gradually propagating into longer cracks that eventually led to the complete failure of the specimens.

Figure 4. Failure modes of Group 1 specimens: (a) Cy-L-FCS-Con; (b) Cy-L-FCS-2BFRP; (c) Cy-L-FCS-4BFRP; (d) Cy-L-FCS-6BFRP; (e) Cy-M-FCS-Con Cy-M-FCS-2BFRP; (f) Cy-M-FCS-4BFRP; (g) Cy-M-FCS-6BFRP; (h) Cy-H-FCS-Con; (i) Cy-H-FCS-2BFRP; (j) Cy-H-FCS-4BFRP; and (k)Cy-H-FCS-6BFRP.

DOI: https://doi.org/10.17509/ajse.v6i1.89929
p- ISSN 2776-6098 e- ISSN 2776-5938

Specimens confined with BFRP jackets exhibited delayed failure compared to their unconfined counterparts. The failure sequence in the confined specimens typically began with the tensile rupture of the BFRP layers, which was subsequently followed by the sudden crushing of the concrete core.

This pattern of behavior suggests that the BFRP jackets were effective in restraining the brittle nature of concrete until the tensile limit of the confinement was exceeded. Observations also indicated that the inner layers of BFRP tended to fail before the outer layers, as evidenced by rupture sounds occurring before the fracture of the outermost wraps. Comparable failure mechanisms have been reported in previous studies [47].

Figure 5. Failure types of Group 2 cylinders: (a) Cy-L-FCH-Con; (b) Cy-L-FCH-2BFRP; (c) Cy-L-FCH-4BFRP; (d) Cy-FCH-6BFRP; (e) Cy-M-FCH-Con; (f) Cy-M-FCH-2BFRP; (g) Cy-M-FCH-4BFRH; (h) Cy-M-FCH-6BFRP; (i) Cy-H-FCH-Con; (j) Cy-H-FCH-2BFRP; (k) Cy-H-FC-4BFRP; (l) Cy-H-FCH-6BFRP.

3.2. Load Vs. Strain Response

The characteristic stress-strain behavior of BFRP-confined concrete is illustrated in **Figure 6**, while the load–axial shortening responses for all specimen groups are shown in **Figure 7**. We showed load-deformation curves of all specimens in **Figures 7(a), 7(b), 7(c), 7(d), 7(e),** and **7(f)** for Subgroup I, Subgroup II, Subgroup III, Subgroup IV, Subgroup V, and Subgroup VI, respectively.

The average axial strain was calculated using displacement transducers placed along the full height of each specimen, following established experimental practices [53, 54]. In contrast to strain gauges, which measure localized strain, displacement transducers capture the overall deformation, thereby justifying the use of the term “average strain” throughout this

DOI: https://doi.org/10.17509/ajse.v6i1.89929
p- ISSN 2775-6793 e- ISSN 2775-6815

study to distinguish it from localized strain measurements. The resulting load–deformation curves exhibited a parabolic profile, with an initial stiff linear branch followed by a gradual transition to a less stiff segment, as illustrated in **Figure 6**.

Both compressive strength and ultimate average strain increased proportionally with the number of BFRP layers. Control specimens in all subgroups failed in a brittle manner, exhibiting little to no ductility. In contrast, specimens confined with BFRP showed significant improvements in ductility, particularly those wrapped with six layers.

Additionally, confined specimens demonstrated consistently higher initial stiffness than unstrengthened specimens, with the degree of improvement increasing alongside the number of BFRP layers. A notable strain-hardening branch was also observed in the stress–strain curves of confined concrete. Similar behavior has been documented in previous studies [44].

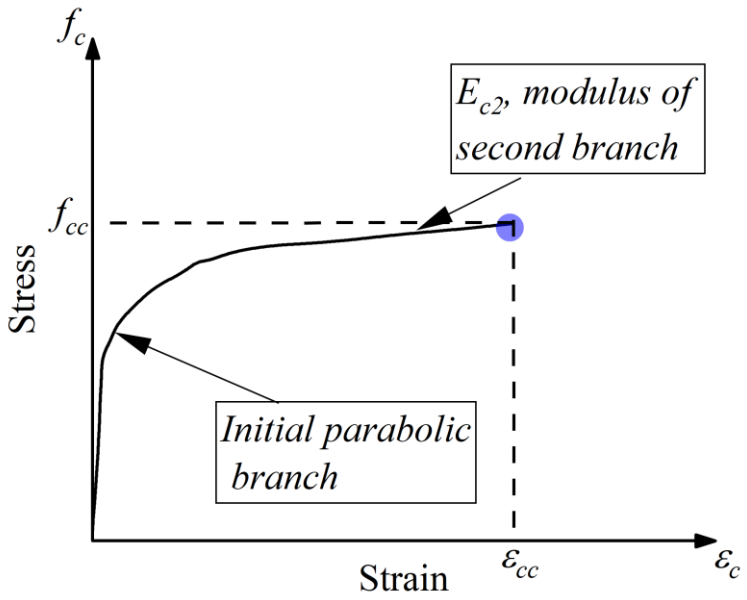

Figure 6. Characteristic shape of stress vs strain curve.

3.3. Peak Stress and Ultimate Average Strain

Table 4 presents a summary of the compressive strength (peak stress), ultimate average strain, and their respective improvements resulting from BFRP confinement. Significant enhancements were observed across all specimen groups.

Subgroups I, II, III, IV, V, and VI demonstrated increases in compressive strength of up to 395.5, 268.8, 210.4, 339.2, 278.3, and 189.2%, respectively. Likewise, the ultimate average strain improved by 583.3, 426.3, 373.7, 301.2, 229.0, and 172.7% in the corresponding subgroups.

The number of BFRP layers was found to be a critical factor influencing mechanical performance. In Subgroup I, the use of two, four, and six layers led to strength enhancements of 188.3, 297.3, and 395.5%, respectively. These results confirm a direct positive correlation between the number of confinement layers and improvements in both strength and ductility. Compared to previous research, which reported compressive strength increases ranging from 20 to 71% and strain improvements between 49 and 296%, the present study achieved substantially higher values. This discrepancy is primarily due to the greater number of BFRP layers applied in the current investigation, which extended up to six layers [44].

DOI: https://doi.org/10.17509/ajse.v6i1.89929
p- ISSN 2776-6098 e- ISSN 2776-5938

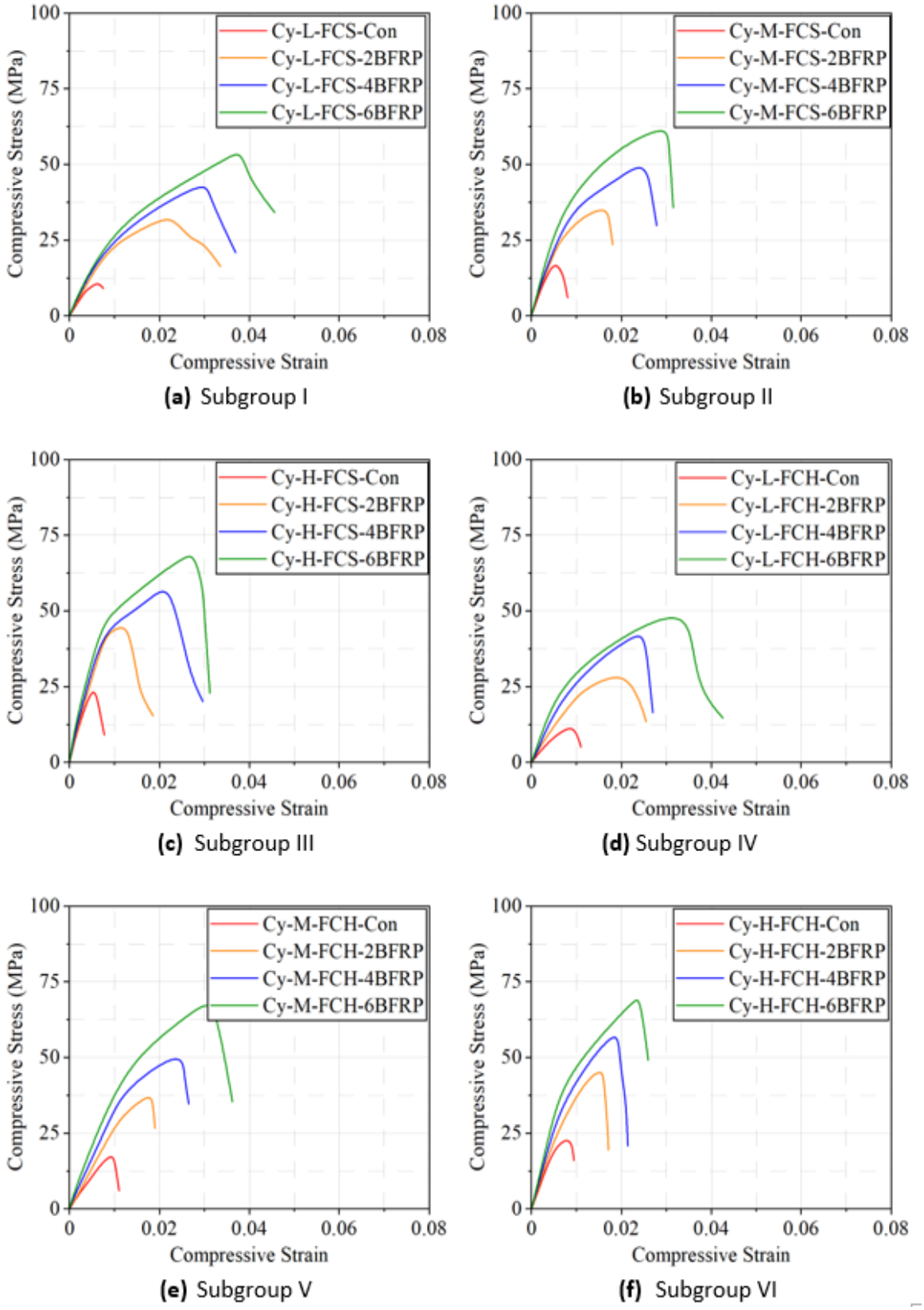

Figure 7. Load-deformation curves of all specimens: (a) Subgroup I; (b) Subgroup II; (c) Subgroup III; (d) Subgroup IV; (e) Subgroup V; and (f) Subgroup VI.

DOI: https://doi.org/10.17509/ajse.v6i1.89929
p- ISSN 2775-6793 e- ISSN 2775-6815

Table 4. Details of ultimate strength, average strain, and their enhancements.

Specimen ID	Ultimate Strength (MPa)	Improvement in Strength (%)	Ultimate Average strain	Improvement in Strain (%)
Cy-L-FCS-Con	11.1	-	0.0060	-
Cy-L-FCS-2BFRP	32.0	188.3	0.0207	245.0
Cy-L-FCS-4BFRP	44.1	297.3	0.0300	400.0
Cy-L-FCS-6BFRP	55.0	395.5	0.0383	583.3
Cy-M-FCS-Con	17.0	-	0.0057	-
Cy-M-FCS-2BFRP	37.0	117.8	0.0168	194.7
Cy-M-FCS-4BFRP	51.6	203.5	0.0253	343.9
Cy-M-FCS-6BFRP	62.7	268.8	0.0300	426.3
Cy-H-FCS-Con	22.0	-	0.0055	-
Cy-H-FCS-2BFRP	45.0	104.5	0.0126	129.1
Cy-H-FCS-4BFRP	58.2	164.5	0.0217	294.5
Cy-H-FCS-6BFRP	68.3	210.4	0.0260	373.7
Cy-L-FCH-Con	12.0	-	0.0085	-
Cy-L-FCH-2BFRP	30.8	156.7	0.0207	143.5
Cy-L-FCH-4BFRP	43.0	258.3	0.0250	194.1
Cy-L-FCH-6BFRP	52.7	339.2	0.0341	301.2
Cy-M-FCH-Con	18.0	-	0.0093	-
Cy-M-FCH-2BFRP	38.0	111.1	0.0177	90.3
Cy-M-FCH-4BFRP	52.9	193.9	0.0250	168.8
Cy-M-FCH-6BFRP	68.1	278.3	0.0306	229.0
Cy-H-FCH-Con	24.0	-	0.0088	-
Cy-H-FCH-2BFRP	46.0	91.7	0.0155	76.1
Cy-H-FCH-4BFRP	58.8	145	0.0190	115.9
C-HS-CBB-6BFRP	69.4	189.2	0.0240	172.7

3.4. Impact of unconfined compressive strength

Table 4 indicates that the enhancement in compressive strength was influenced by the unconfined compressive strength of the specimens. This relationship is graphically presented in **Figure 8**. The efficiency of BFRP confinement in improving compressive strength decreased as the unconfined compressive strength increased. For instance, specimens confined with two BFRP layers and possessing medium and high unconfined strengths exhibited 70.5 and 117.8% lower improvements in compressive strength, respectively, compared to those with low unconfined strength. This observation was consistent across both groups, suggesting that the type of recycled brick aggregate did not alter the trend of reduced confinement efficiency with increasing unconfined compressive strength. A similar behavior was also observed for the ultimate average strain, as illustrated in **Figure 9**.

3.5. Effect of Recycled Brick Type

Two types of recycled bricks, namely fired-clay solid (FCS) and fired-clay hollow (FCH), were used in this study as substitutes for natural coarse aggregates. As summarized in **Table 4**, the type of recycled brick had a significant effect on the efficiency of BFRP confinement. Specimens in Group 1, which incorporated FCS aggregates, exhibited greater enhancements in both compressive strength and ultimate average strain compared to those in Group 2, which used FCH aggregates. This difference is attributed to the inherently lower compressive strength of FCS bricks, which allowed for more effective confinement and greater structural improvement when wrapped with BFRP.

DOI: https://doi.org/10.17509/ajse.v6i1.89929
p- ISSN 2776-6098 e- ISSN 2776-5938

Figure 10 provides a comparative visualization of the influence of recycled brick type across different strength levels. **Figure 10(a)** shows that for specimens with low unconfined strength, those containing FCS aggregates achieved markedly higher compressive strength gains than their FCH counterparts, with increases of 31.6, 39.0, and 56.3% for the two, four, and six BFRP layer configurations, respectively. **Figure 10(b)** illustrates the trend for medium-strength concrete, where FCS specimens again outperformed FCH specimens, though the margin of improvement was slightly reduced. Similarly, **Figure 10(c)** presents the results for high-strength specimens, confirming that the advantage of using FCS aggregates in combination with BFRP confinement persisted across all strength levels. This consistent pattern further supports the conclusion that the mechanical properties of the recycled brick type play a decisive role in the overall effectiveness of the confinement strategy (as evidenced in **Table 4** and **Figure 10**).

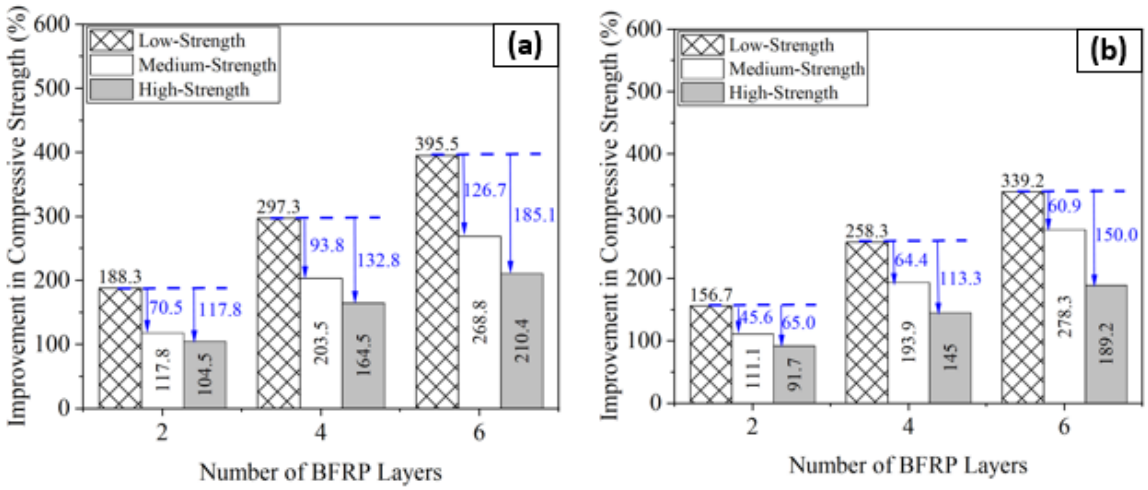

Figure 8. Comparison of increase in compressive strength of samples with different unconfined strengths (a) Group 1 and (b) Group 2.

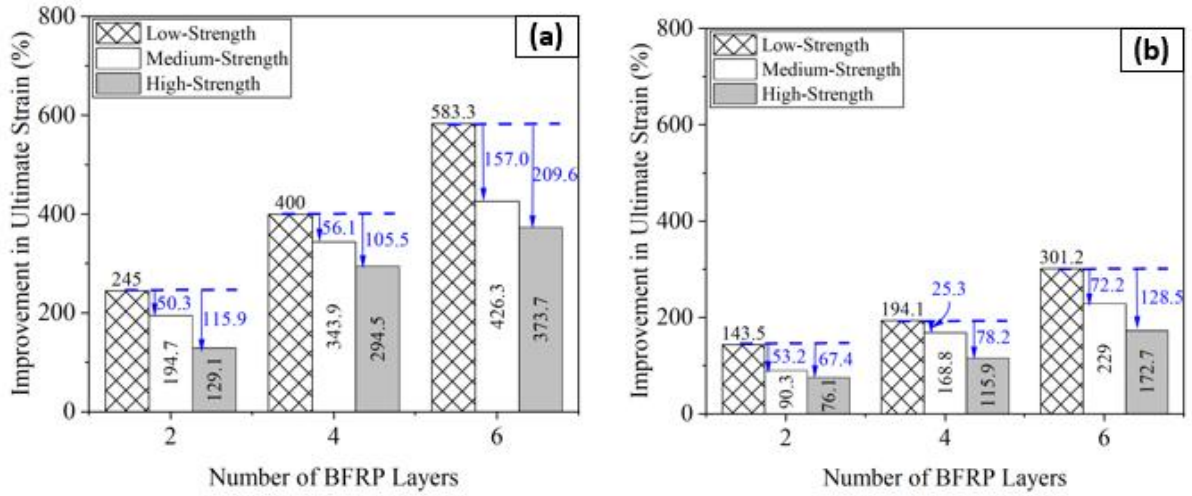

Figure 9. Comparison of improvement in ultimate average strain of specimens with different unconfined strengths (a) Group 1 and (b) Group 2.

DOI: https://doi.org/10.17509/ajse.v6i1.89929
p- ISSN 2775-6793 e- ISSN 2775-6815

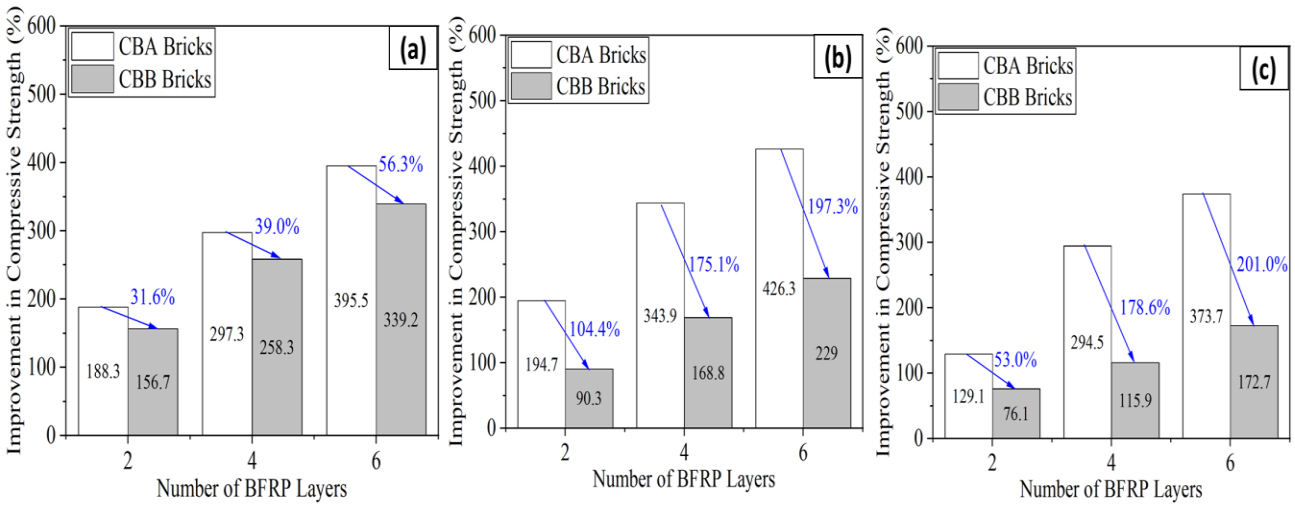

Figure 10. Comparison of the increase in peak stress (compressive strength) of concrete with different recycled bricks: (a) low unconfined strength, (b) medium unconfined strength, and (c) high unconfined strength.

3.6. Evaluation of Current FRP-confined Concrete Expressions

3.6.1. Existing Ultimate Strength Models for FRP-confined Concrete

Numerous expressions have been proposed in the literature to establish a relationship between external passive confinement and the enhancement of concrete's mechanical properties [54, 55]. Typically, the influence of external confinement is quantified as a function of the lateral pressure generated during the expansion of concrete. This lateral pressure can be expressed as a function of the increase in compressive strength, as shown in Equation (1) :

$$\frac{f_{cc}}{f_{co}} = 1 + k_1 \left(\frac{f_l}{f_{co}}\right)^{k_2} \quad (1)$$

Where f_l represents the external passive confinement pressure exerted by FRP confinement, f_{cc} represents the compressive strength of FRP-confined concrete, f_{co} represents the unconfined compressive strength, and k_1 and k_2 are constants of regression.

The outer lateral pressure may be established by attaining equilibrium among internal pressure and the subsequent confining stresses with BFRP layers, as illustrated in **Figure 11**. Confining action of BFRP wrap on concrete in the core (**Figure 11(a)**) and BFRP wrap (**Figure 11(b)**) are presented [56]. Then, it is precisely represented in Equation (2) [56]:

$$f_l = \frac{2n_f f_f t_f}{D} \quad (2)$$

Where f_f and D are the fracture capacity of BFRP wraps and the diameter of the specimen, respectively, n_f represents the quantity of BFRP layers, and t_f represents the thickness of one BFRP layer.

It is noted that f_f is not reduced to account for the premature fracture, as reported by earlier studies. However, future studies should address this issue by measuring the strain of BFRP throughout the loading history.

DOI: https://doi.org/10.17509/ajse.v6i1.89929
p- ISSN 2776-6098 e- ISSN 2776-5938

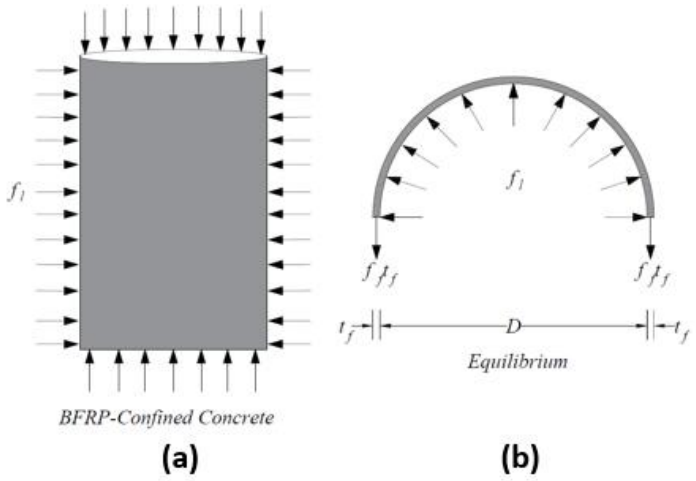

Figure 11. Confining action of BFRP wrap on concrete (a) concrete core and (b) BFRP wrap [62].

3.6.2. Current ultimate strain expressions for FRP-confined concrete

The conventional approach employs the structure of Equation (3) to establish a correlation between the ultimate strain of confined concrete and the magnitude of the applied external lateral pressure [23, 57, 58]:

$$\frac{\epsilon_{cc}}{\epsilon_{co}} = 1 + k_3 \left(\frac{f_l}{f_{co}}\right)^{k_4} \tag{3}$$

Where ϵ_{cc} denotes the ultimate strain of confined cylinders, while ϵ_{co} refers to the ultimate strain of unconfined cylinders. In this study, the applicability of existing ultimate strain expressions is assessed under the assumption that confinement provided by BFRP wraps is analogous to conventional FRP confinement techniques. **Table 5** summarizes a set of ultimate stress and strain expressions specifically developed for externally confined concrete cylinders.

Table 5. Current compressive strength and strain models.

No.	Study	Compressive Strength f_{cc}	Ultimate Strain ϵ_{cc}
1	Ghernouti and Rabehi [59]	$\frac{f_{cc}}{f_{co}} = 1 + 2.038\frac{f_l}{f_{co}}$	$\frac{\epsilon_{cc}}{\epsilon_{co}} = 1 + 10.56\left(\frac{f_l}{f_{co}}\right)$
2	Benzaid et al. [60]	$\frac{f_{cc}}{f_{co}} = 1 + 2.20\frac{f_l}{f_{co}}$	$\frac{\epsilon_{cc}}{\epsilon_{co}} = 2 + 7.6\left(\frac{f_l}{f_{co}}\right)$
3	Bisby et al. [61]	$\frac{f_{cc}}{f_{co}} = 1 + 2.425\frac{f_l}{f_{co}}$	-
4	Wu et al. [62]	$\frac{f_{cc}}{f_{co}} = 1 + 3.20\frac{f_l}{f_{co}}$	$\frac{\epsilon_{cc}}{\epsilon_{co}} = 1 + 9.5\left(\frac{f_l}{f_{co}}\right)$
5	Teng et al. [63]	$\frac{f_{cc}}{f_{co}} = 1 + 3.50\frac{f_l}{f_{co}}$	$\frac{\epsilon_{cc}}{\epsilon_{co}} = 1 + 17.5\left(\frac{f_l}{f_{co}}\right)^{1.2}$
6	Ahmad and Shah [64]	$\frac{f_{cc}}{f_{co}} = 1 + 4.2556\frac{f_l}{f_{co}}$	-
7	Hussain et al. [65]	$\frac{f_{cc}}{f_{co}} = 1 + 6.40\frac{f_l}{f_{co}}$	-
8	Karbhari and Gao [66]	$\frac{f_{cc}}{f_{co}} = 1 + 2.1\left(\frac{f_l}{f_{co}}\right)^{0.87}$	-

DOI: https://doi.org/10.17509/ajse.v6i1.89929
p- ISSN 2775-6793 e- ISSN 2775-6815

3.6.3. Evaluation of Current Ultimate Strength and Strain Expressions

Previous studies [53–55] have proposed several advanced confinement models that incorporated hoop strain as a key parameter. However, in this study, hoop strain was not measured due to budgetary limitations. The term *ff* corresponds to the fracture capacity of BFRP wraps. The performance of the existing models listed in **Table 5** for predicting ultimate compressive strength is illustrated in **Figure 12**.

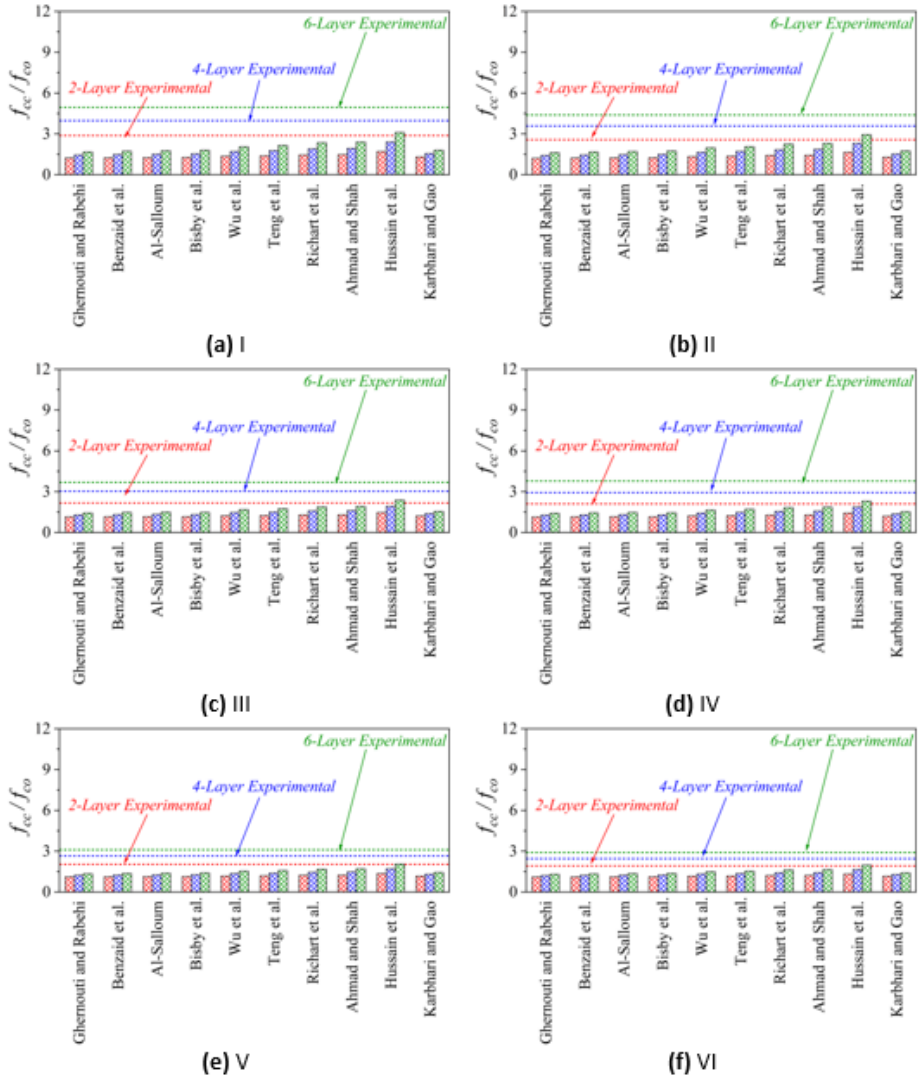

Figure 12. Comparison of the predicted normalized ultimate strengths by existing models with experimental results: (a) I; (b) II; (c) III; (d) IV; (e) V; and (f) VI.

It is evident that the current expressions significantly underestimate the ultimate compressive strength, thereby underrepresenting the efficiency of BFRP wraps in enhancing the compressive strength of ReBAC. This tendency was consistently observed across all six subgroups, underscoring the necessity of developing distinct analytical expressions for predicting the compressive strength of BFRP-confined ReBAC. A similar observation was made for ultimate compressive strain, as depicted in **Figure 13** for Subgroup I. Consequently, the

DOI: https://doi.org/10.17509/ajse.v6i1.89929
p- ISSN 2776-6098 e- ISSN 2776-5938

following sections introduce a regression-based approach for predicting both the compressive strength and the ultimate strain of BFRP-confined ReBAC.

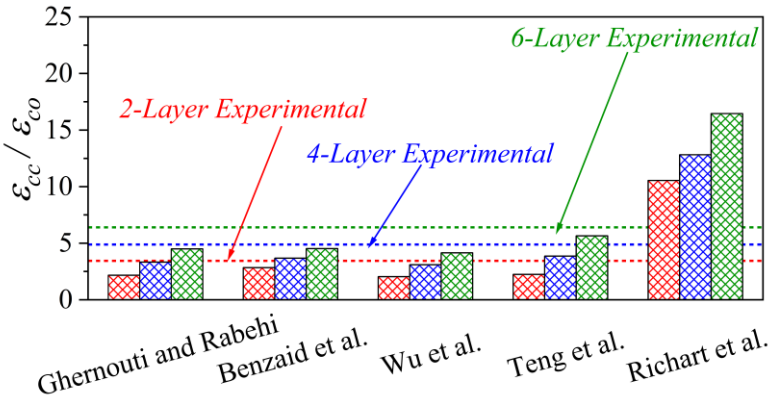

Figure 13. Comparison of the predicted normalized ultimate average strains by existing models with experimental results of Subgroup I.

3.7. Proposed Models for Ultimate Strength and Average Strain

Based on the findings of this study, an equation similar in form to Equation (1) is proposed for predicting the compressive strength of BFRP-confined ReBAC. As shown in **Table 4**, the enhancement in both compressive strength and ultimate average strain was influenced by the type of recycled brick aggregates.

Accordingly, the recycled brick type was incorporated as an explanatory variable in the regression model through its compressive strength (*fbc*, MPa). A nonlinear regression analysis was performed using the classical Gauss–Newton algorithm, yielding the following expression in Equation (4).

$$\frac{f_{cc}}{f_{co}} = 1 + 8.864\left(\frac{f_l}{f_{co}}\right)^{0.768}\left(\frac{f_{bc}}{f_{co}}\right)^{0.003} \quad (MPa) \tag{4}$$

It is noteworthy that Equation (4) achieved a coefficient of determination (R^2) of 0.97, indicating an excellent correlation with the experimental data, as illustrated in **Figure 14(a)**. Similarly, an equation analogous to Equation (3) is proposed for predicting the ultimate average strain, expressed as Equation (5):

$$\frac{\epsilon_{cc}}{\epsilon_{co}} = 1 + 6.493\left(\frac{f_l}{f_{co}}\right)^{0.929}\left(\frac{f_{bc}}{f_{co}}\right)^{630} \tag{5}$$

Equation (5) yielded a coefficient of determination (R^2) of 0.90, which also demonstrates a strong agreement between the experimental ultimate average strain and the corresponding predicted values, as illustrated in **Figure 14(b)**.

DOI: https://doi.org/10.17509/ajse.v6i1.89929
p- ISSN 2775-6793 e- ISSN 2775-6815

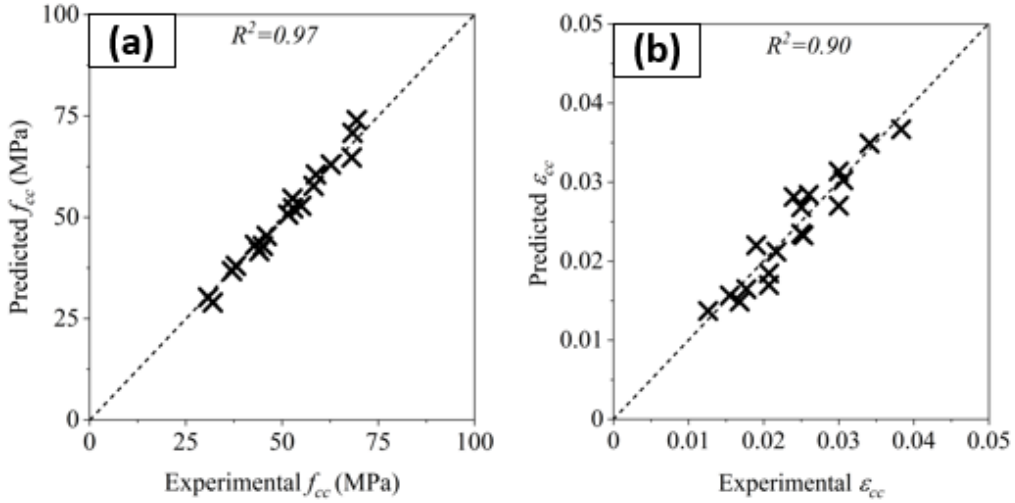

Figure 14. Comparison of predicted and experimental (a) compressive strength and (b) ultimate average strain.

3.8. Prediction of Compressive Stress versus Strain Curves

The experimental compressive stress–strain curves exhibited an initial linear or quasi-linear segment, followed by a parabolic ascending branch. Richard and Abbott [67] previously proposed a design-oriented model to describe similar stress–strain behavior. Their four-parameter approach has since been widely adopted for modeling the stress–strain response of FRP-confined concrete. In this model, the stress–strain relationship is governed by two distinct moduli: one representing the elastic portion of the initial ascending branch (*Ec1*), and the other corresponding to the initial slope of the post-peak branch (*Ec2*), as expressed in Equations (6) and (7). A polynomial constant (*n*) is employed within these curves to provide a smooth transition between the two segments.

$$f_c = \frac{(E_{c1} - E_{c2})\epsilon_c}{\left[1 + \left\{\frac{(E_{c1} - E_{c2})\epsilon_c}{f_{cc} - E_{c2}\epsilon_{cc}}\right\}^n\right]^{\frac{1}{n}}} + E_{c2}\epsilon_c \quad (6)$$

$$n = 1.0 + \frac{1.0}{\frac{E_{c1}}{E_{c2}} - 1.0} \quad (7)$$

Where *fc* denotes the stress corresponding to an arbitrary strain ϵ_c. Regression-based expressions are proposed to predict the slopes E_{c1} and E_{c2}. From the experimental results, it was observed that the elastic modulus increased in the strengthened concrete, with further improvement corresponding to the greater number of BFRP layers. Accordingly, a nonlinear regression analysis based on the Gauss–Newton algorithm was performed, resulting in the following expression for the elastic modulus of BFRP-confined ReBAC (equation (8)).

$$E_{c1} = 344.254 \times \left(\frac{f_l}{f_{co}}\right)^{0.359} \times \left(\frac{f_{co}}{f_{bc}}\right)^{0.012} \times (f_{co})^{1.143} \quad (MPa) \quad (8)$$

The statistical reliability of Equation (8) is reflected in its coefficient of determination (R^2) of 0.94, as illustrated in **Figure 15(a)**. From the experimental stress–strain responses, it was observed that the slope of the second branch within a given subgroup exhibited minimal variation. Therefore, an average value was adopted for each subgroup. Consequently, the

DOI: https://doi.org/10.17509/ajse.v6i1.89929
p- ISSN 2776-6098 e- ISSN 2776-5938

number of BFRP layers was not considered in the regression analysis for the stiffness of the second branch of the stress–strain curves (*Ec2*). The resulting equation showed close agreement with the experimental results. The statistical reliability of Equation (9) is confirmed by its R^2 value of 0.87, as shown in **Figure 15(b)**.

$$E_{c2} = 144.749 \times \left(\frac{f_{bc}}{f_{co}}\right)^{0.070} \times (f_{co})^{0.740} \quad (MPa) \tag{9}$$

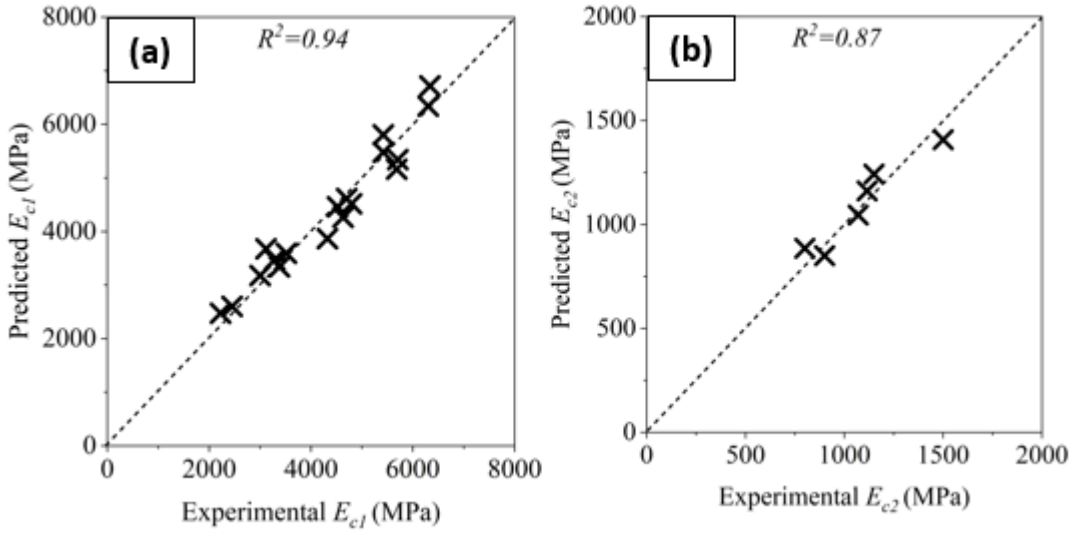

Figure 15. Comparison of predicted and experimental (a) E_{c1} and (b) E_{c2}.

Figures 16 and 17 present comparisons between the predicted and experimental compressive stress–strain curves for Group 1 and Group 2 specimens, respectively. The predicted curves were truncated at the ultimate strain values derived from the regression model (Equation (5)), while the corresponding compressive strengths were calculated using Equation (4). Both the elastic modulus (E_{c1}) and the hardening modulus (E_{c2}) were obtained from the proposed predictive expressions. In general, the predicted stress–strain curves aligned closely with the experimental data, demonstrating the robustness of the proposed nonlinear modeling approach for BFRP-confined recycled brick aggregate concrete (ReBAC). A notable deviation was observed for the specimen Cy-H-FCH-2BFRP, where the predicted stress–strain response underestimated the experimental behavior. Nevertheless, for all other cases, the model predictions were consistent with the experimental results.

Figure 16 illustrates the response of specimens in Group 1 (fired-clay solid bricks). Specifically, **Figures 16(a)** through **16(c)** show the stress–strain behavior of low-strength specimens confined with two, four, and six layers of BFRP (Cy-L-FCS-2BFRP, Cy-L-FCS-4BFRP, and Cy-L-FCS-6BFRP). These curves reveal a consistent improvement in ductility and peak stress as the number of layers increases. **Figures 16(d)** through **16(f)** display the curves for medium-strength specimens (Cy-M-FCS-2BFRP to Cy-M-FCS-6BFRP), with similar upward trends in both strength and strain capacity. **Figures 16(g)** through **16(i)** represent high-strength specimens, where the confinement effect, while still evident, is less pronounced due to the inherently higher unconfined strength.

Figure 17 presents the curves for Group 2 specimens using fired-clay hollow bricks. **Figures 17(a)** through **(c)** correspond to low-strength mixes with two to six layers of BFRP (Cy-L-FCH-2BFRP to Cy-L-FCH-6BFRP). These curves demonstrate gradual increases in ductility and peak

DOI: https://doi.org/10.17509/ajse.v6i1.89929
p- ISSN 2775-6793 e- ISSN 2775-6815

stress, although the confinement effect is somewhat less significant than in Group 1. **Figures 17(d)** through **(f)** show medium-strength specimens (Cy-M-FCH-2BFRP to Cy-M-FCH-6BFRP), where the predicted and experimental curves remain closely aligned. **Figures 17(g)** through **17(i)** cover high-strength specimens (Cy-H-FCH-2BFRP to Cy-H-FCH-6BFRP), including the one notable outlier, **Figure 17(g)**, where underestimation of experimental response occurred. Overall, the consistency between predicted and measured responses across these figures supports the validity of the proposed stress–strain modeling approach for different concrete strengths and brick types.

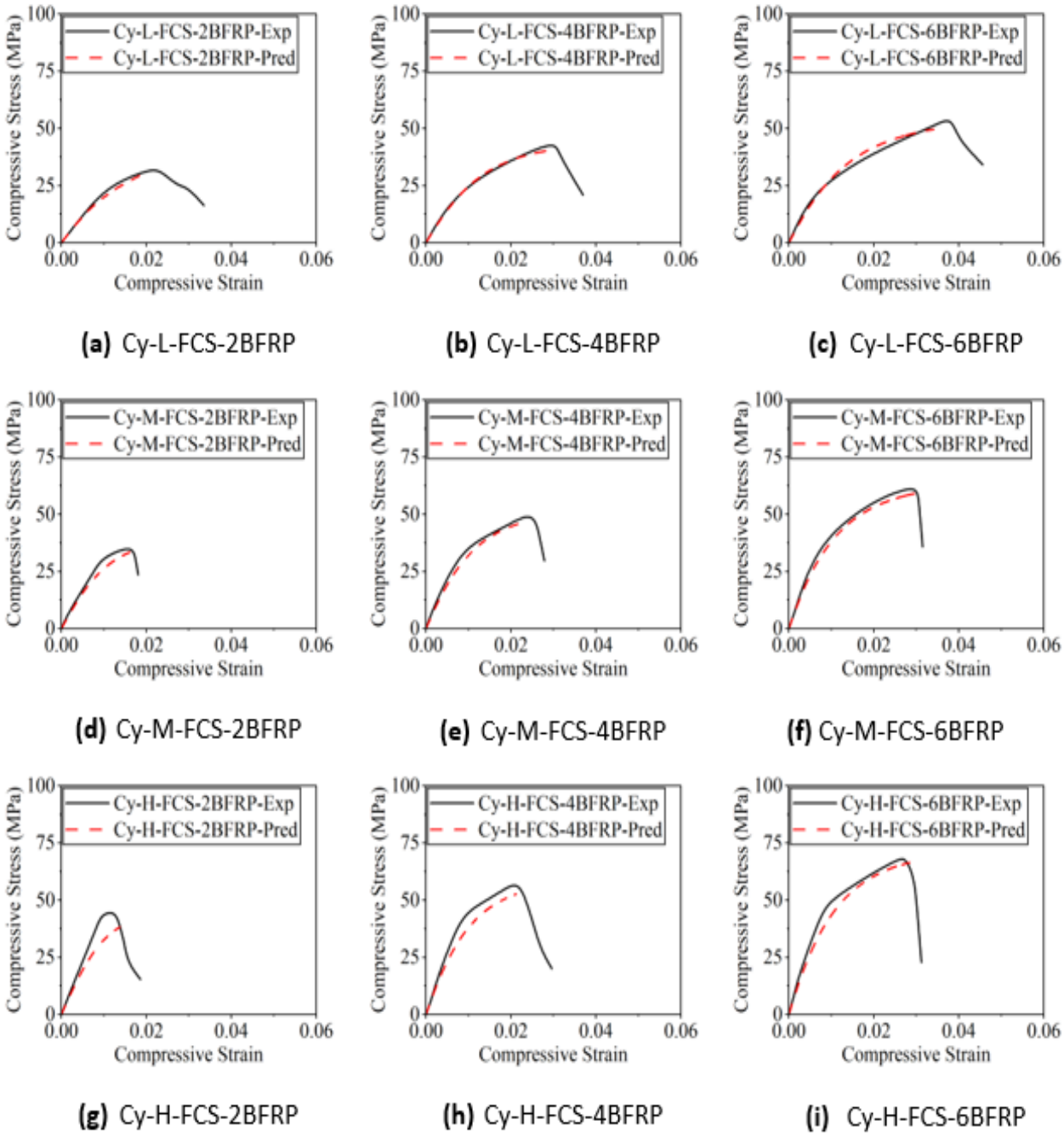

Figure 16. Comparison of predicted and experimental stress vs. strain curves of specimens in Group 1: (a) Cy-L-FCS-2BFRP, (b) Cy-L-FCS-4BFRP, (c) Cy-L-FCS-6BFRP, (d) Cy-M-FCS-2BFRP, (e) Cy-M-FCS-4BFRP, (f) Cy-M-FCS-6BFRP, (g) Cy-H-FCS-2BFRP, (h) Cy-H-FCS-4BFRP, and (i) Cy-H-FCS-6BFRP.

DOI: https://doi.org/10.17509/ajse.v6i1.89929
p- ISSN 2776-6098 e- ISSN 2776-5938

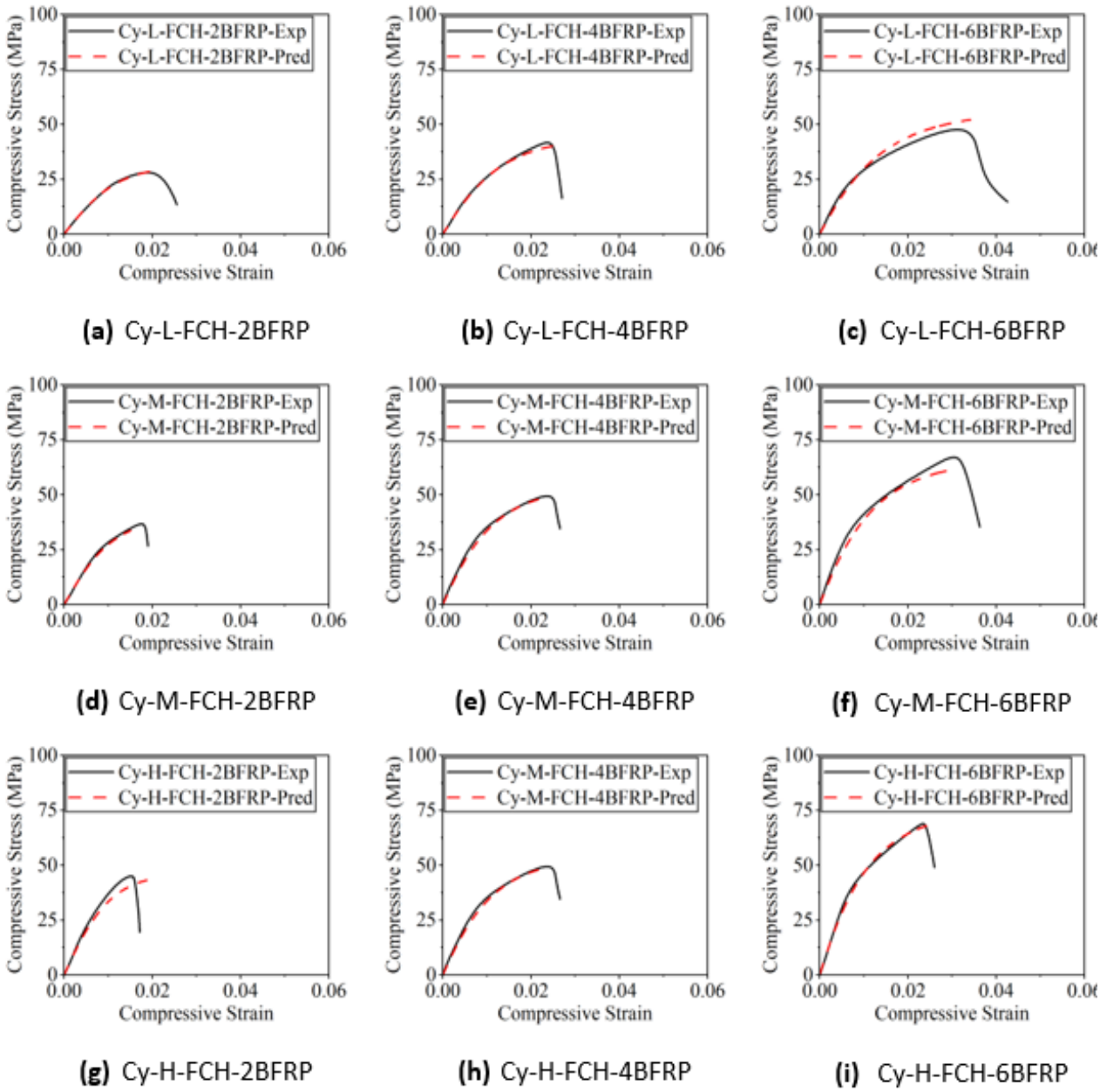

Figure 17. Comparison of predicted and experimental stress vs. strain curves of specimens in Group 2: (a) Cy-L-FCS-2BFRP, (b) Cy-L-FCS-4BFRP, (c) Cy-L-FCS-6BFRP, (d) Cy-M-FCS-2BFRP, (e) Cy-M-FCS-4BFRP, (f) Cy-M-FCS-6BFRP, (g) Cy-H-FCS-2BFRP, (h) Cy-H-FCS-4BFRP, and (i) Cy-H-FCS-6BFRP

This study aimed to investigate the mechanical behavior of recycled brick aggregate concrete (ReBAC) confined with basalt fiber-reinforced polymer (BFRP) jackets, and to evaluate the predictive performance of regression-based models for strength and stress–strain response. The discussion in this section integrates key findings and offers critical interpretations in relation to confinement effectiveness, aggregate type, concrete strength level, and modeling accuracy. Several important points are in the following:

(i) Effectiveness of BFRP Confinement. The experimental results clearly demonstrate that BFRP confinement significantly improves both compressive strength and ductility of ReBAC. As shown in Table 4, all confined specimens exhibited increased peak strength

DOI: https://doi.org/10.17509/ajse.v6i1.89929
p- ISSN 2775-6793 e- ISSN 2775-6815

and ultimate average strain compared to their unconfined counterparts. The magnitude of improvement was directly related to the number of BFRP layers, with six-layer configurations yielding the highest enhancement. This confirms the ability of BFRP jackets to delay brittle failure and induce strain hardening in confined concrete elements. The observed increase in initial stiffness and presence of a second ascending branch in the stress–strain curves (**Figure 6**) further support the effectiveness of confinement in modifying failure mechanisms.

(ii) Influence of Brick Type on Confinement Efficiency. The type of recycled brick aggregate was found to be a critical variable in determining the confinement efficiency of BFRP. As indicated in **Table 4** and **Figure 10**, specimens incorporating fired-clay solid (FCS) bricks consistently outperformed those with fired-clay hollow (FCH) bricks across all strength levels. This difference is attributed to the lower inherent compressive strength of FCS aggregates, which likely allowed the BFRP jackets to mobilize higher confinement pressure. Consequently, greater energy absorption and deformation capacity were achieved in Group 1 specimens. This finding implies that selecting weaker recycled aggregates, within structurally acceptable limits, may enhance the efficacy of external confinement systems.

(iii) Role of Unconfined Compressive Strength. The confinement efficiency of BFRP was inversely related to the unconfined compressive strength of the concrete matrix. As concrete strength increased from low to high, the relative gains in both compressive strength and ductility due to confinement decreased. This trend, visible in the comparative data for Subgroups I to III and IV to VI, is in line with the theoretical understanding that lower-strength concretes are more responsive to external confinement due to their lower internal stiffness and higher deformability. Therefore, the use of BFRP confinement may be particularly advantageous for structural elements utilizing lower-grade or recycled concrete.

(iv) Accuracy and Limitations of the Predictive Model. The proposed regression-based model demonstrated strong agreement with experimental results, as shown in **Figures 16 and 17**. Most predicted stress-strain curves closely matched the experimental responses in terms of shape, peak stress, and ultimate strain. The good fit, especially for specimens with two to six BFRP layers, indicates that the modeling approach is reliable for capturing the nonlinear behavior of confined ReBAC. However, a notable exception was observed in the case of specimen Cy-H-FCH-2BFRP, where the model underestimated the stress–strain response. This deviation may stem from variability in material properties or local defects in specimen preparation, and suggests that further refinement of the model is needed to improve robustness across all conditions. The predictive equations used to estimate compressive strength and strain (Equations (4) and (5)), as well as the moduli of elasticity (Ec1) and strain-hardening branch (Ec2), yielded high coefficients of determination (R^2), indicating statistical validity. Nonetheless, the model was developed using a limited dataset, confined to a specific range of concrete strengths and aggregate types. As such, its applicability should be restricted to the experimental domain of this study. Broader validation through expanded datasets and inclusion of additional material variables (such as fiber orientation, bonding quality, and environmental conditions) is recommended for future research.

(v) Implications for Sustainable Construction. From a sustainability perspective, the findings underscore the feasibility of combining recycled brick aggregates and natural fiber-based composites for structural enhancement. The use of ReBAC reduces the dependency on virgin aggregates, while BFRP (being environmentally friendly and produced without

DOI: https://doi.org/10.17509/ajse.v6i1.89929
p- ISSN 2776-6098 e- ISSN 2776-5938

chemical additives) presents a low-impact alternative to synthetic FRPs. These attributes align well with the goals of sustainable development, particularly in promoting responsible consumption and production (SDG 12) and fostering resilient infrastructure (SDG 9). The practical integration of these materials in structural applications contributes to circular economy practices in the construction sector.

4. CONCLUSION

To enable the structural use of recycled brick aggregates in concrete, supplementary confinement is essential. This study investigated the effectiveness of BFRP sheets in enhancing the performance of ReBAC, considering the influence of the number of BFRP layers, unconfined compressive strength, and brick type (fired-clay solid vs. fired-clay hollow). A total of 18 specimen types were tested across six subgroups, leading to the following conclusions:

(i) Failure behavior: BFRP confinement significantly improved the failure characteristics of ReBAC. Reinforced specimens failed later than unconfined ones, with failure initiated by rupture of the BFRP jackets, followed by concrete crushing. This indicates that BFRP jackets effectively delayed brittle failure by sustaining tensile demands.

(ii) Load–deformation response: Control specimens exhibited an initial parabolic branch followed by a sudden loss in capacity. In contrast, BFRP-confined specimens displayed enhanced ductility, characterized by an additional ascending second branch.

(iii) Strength and strain enhancement: BFRP confinement resulted in remarkable gains in compressive strength and ultimate strain. Strength improvements reached up to 395% and 339% for solid and hollow brick concretes, respectively, while ultimate strains increased by as much as 583% and 301%. These improvements diminished as the unconfined compressive strength increased, highlighting the greater effectiveness of BFRP in lower-strength concretes. The large enhancements reported here, exceeding prior studies, are attributed to the higher number of BFRP layers used (up to six).

(iv) Limitations of existing models: Existing models for FRP-confined concrete underestimated the compressive strength and ultimate strain of BFRP-confined ReBAC, underscoring the need for new, tailored models.

(v) Proposed design-oriented model: This study developed regression-based expressions for key parameters, including elastic modulus, second-branch modulus, compressive strength, and ultimate strain. Integrated with an existing stress–strain framework, these expressions enabled accurate predictions of the compressive stress–strain behavior, with coefficients of determination approaching unity. The proposed procedure demonstrated strong agreement with experimental results, though validation against broader datasets is still required.

Overall, this research highlights the potential of BFRP sheets as an effective means to strengthen ReBAC for structural applications. The proposed design-oriented model offers a novel and practical approach for predicting the compressive behavior of BFRP-confined ReBAC. Nonetheless, future studies should aim to validate and refine the model using larger datasets, additional brick sources, and advanced modeling techniques to further enhance its generalizability.

5. AUTHORS' NOTE

The authors declare that there is no conflict of interest regarding the publication of this article. Authors confirmed that the paper was free of plagiarism.

DOI: https://doi.org/10.17509/ajse.v6i1.89929
p- ISSN 2775-6793 e- ISSN 2775-6815

6. ACKNOWLEDGEMENT

This research is supported by Thailand Science Research and Innovation (TSRI) Fundamental Fund, fiscal year 2025. We also thank the Asian Institute of Technology (AIT), Thailand, for supporting test facilities.

7. REFERENCES

[1] Hua, Z., and Yuanfeng, L. (2019). Probe into the resource utilization of abandoned clay bricks in construction. *Henan Building Materials*, *4*, 167-169.

[2] Xiao, J., Li, W., Fan, Y., and Huang, X. (2012). An overview of study on recycled aggregate concrete in China (1996–2011). *Construction and Building Materials*, *31*, 364-383.

[3] Al-Rousan, R. Z., and Sawalha, H. M. (2024). The behavior of concrete filled steel tubular columns infilled with high-strength geopolymer recycled aggregate concrete. *Steel and Composite Structures*, *51*(6), 661.

[4] Han, Q., Yuan, W. Y., Ozbakkaloglu, T., Bai, Y. L., and Du, X. L. (2020). Compressive behavior for recycled aggregate concrete confined with recycled polyethylene naphthalate/terephthalate composites. *Construction and Building Materials*, *261*, 120498.

[5] Bai, Y. L., Zhang, Y. F., Jia, J. F., Han, Q., and Gao, W. Y. (2022). Compressive behavior of double-skin tubular stub columns with recycled aggregate concrete and a PET FRP jacket. *Construction and Building Materials*, *332*, 127321.

[6] Al-Rousan, R. Z. (2022). Cyclic behavior of alkali-silica reaction-damaged reinforced concrete beam-column joints strengthened with FRP composites. *Case Studies in Construction Materials*, *16*, e00869.

[7] Al-Rousan, R. Z., and Alnemrawi, B. A. R. (2024). Behaviour of thermally shocked RC columns internally confined by auxetic steel wire mesh. *Proceedings of the Institution of Civil Engineers-Structures and Buildings*, *177*(10), 864-877.

[8] Hamad, B. S., and Dawi, A. H. (2017). Sustainable normal and high strength recycled aggregate concretes using crushed tested cylinders as coarse aggregates. *Case Studies in Construction Materials*, *7*, 228-239.

[9] Ohemeng, E. A., and Ekolu, S. O. (2020). Comparative analysis on costs and benefits of producing natural and recycled concrete aggregates: A South African case study. *Case Studies in Construction Materials*, *13*, e00450.

[10] Hameed, A., Rasool, A. M., Ibrahim, Y. E., Afzal, M. F. U. D., Qazi, A. U., and Hameed, I. (2022). Utilization of fly ash as a viscosity-modifying agent to produce cost-effective, self-compacting concrete: A sustainable solution. *Sustainability*, *14*(18), 11559.

[11] Al-Rousan, R. Z. (2022). Cyclic lateral behavior of NLFEA heat-damaged circular CFT steel columns confined at the end with CFRP composites. *Case Studies in Construction Materials*, *17*, e01223.

[12] Al-Rousan, R. Z., Bara'a, R. A., and Sawalha, H. M. (2024). The ultimate capacity of geopolymer recycled aggregate concrete filled steel tubular columns: Numerical and theoretical study. *Journal of Building Engineering*, *96*, 110365.

[13] Alnemrawi, B. A. R., and Al-Rousan, R. (2024). The detailed axial compression behavior of CFST columns infilled by lightweight concrete. *Buildings*, *14*(9), 2844.

[14] Cantero, B., Bravo, M., De Brito, J., Del Bosque, I. S., and Medina, C. (2021). Water transport and shrinkage in concrete made with ground recycled concrete-additioned cement and mixed recycled aggregate. *Cement and Concrete Composites*, *118*, 103957.

[15] Etxeberria, M., Marí, A. R., and Vázquez, E. (2007). Recycled aggregate concrete as structural material. *Materials and structures*, *40*(5), 529-541.

[16] Mefteh, H., Kebaïli, O., Oucief, H., Berredjem, L., and Arabi, N. (2013). Influence of moisture conditioning of recycled aggregates on the properties of fresh and hardened concrete. *Journal of cleaner production*, *54*, 282-288.

[17] Khalaf, F. M., and DeVenny, A. S. (2004). Recycling of demolished masonry rubble as coarse aggregate in concrete. *Journal of Materials in Civil Engineering*, *16*(4), 331-340.

[18] Akhtaruzzaman, A. A., and Hasnat, A. (1983). Properties of concrete using crushed brick as aggregate. *Concrete International*, *5*(2), 58-63.

[19] Khaloo, A. R. (1994). Properties of concrete using crushed clinker brick as coarse aggregate. *Materials Journal*, *91*(4), 401-407.

[20] Khalaf, F. M. (2006). Using crushed clay brick as coarse aggregate in concrete. *Journal of Materials in Civil Engineering*, *18*(4), 518-526.

[21] Zachariah, J. P., Sarkar, P. P., and Nandi, D. (2020). A study on the properties of cement grouted open-graded bituminous concrete with brick as aggregates. *Construction and Building Materials*, *256*, 119436.

[22] Saingam, P., Ejaz, A., Ali, N., Nawaz, A., Hussain, Q., and Joyklad, P. (2023). Prediction of stress–strain curves for HFRP composite confined brick aggregate concrete under axial load. *Polymers*, *15*(4), 844.

[23] Joyklad, P., Saingam, P., Ali, N., Ejaz, A., Hussain, Q., Khan, K., and Chaiyasarn, K. (2022). Low-cost fiber chopped strand mat composites for compressive stress and strain enhancement of concrete made with brick waste aggregates. *Polymers*, *14*(21), 4714.

[24] Al-Rousan, R. (2020). Behavior of circular reinforced concrete columns confined with CFRP composites. *Procedia Manufacturing*, *44*, 623-630.

[25] Al-Rousan, R. Z., and Alnemrawi, B. A. R. (2023). Cyclic behavior of CFRP confined circular CFST damaged by alkali-silica reaction. *International Journal of Civil Engineering*, *21*(7), 1159-1180.

[26] Al-Rousan, R. (2020). Behavior of CFRP strengthened columns damaged by thermal shock. *Magazine of Civil Engineering*, (5 (97)), 9708.

[27] Abdalla, K. M., Al-Rousan, R., Alhassan, M. A., and Lagaros, N. D. (2020). Finite-element modelling of concrete-filled steel tube columns wrapped with CFRP. *Proceedings of the Institution of Civil Engineers-Structures and Buildings*, *173*(11), 844-857.

[28] Jiangfeng, D., Shucheng, Y., Qingyuan, W., Wenyu, Z., Jiangfeng, D., Shucheng, Y., and Wenyu, Z. (2019). Flexural behavior of RC beams made with recycled aggregate concrete and strengthened by CFRP sheets. *Journal of Building Materials and Structures*, *40*, 71-78.

[29] Ahmad, S., Shah, A., Nawaz, A., and Salimullah, K. (2010). Shear strengthening of corbels with carbon fibre reinforced polymers (CFRP). *Materiales de Construcción*, *60*(299), 79-97.

DOI: https://doi.org/10.17509/ajse.v6i1.89929
p- ISSN 2775-6793 e- ISSN 2775-6815

[30] Al-Rousan, R. Z., and Barfed, M. H. (2019). Impact of curvature type on the behavior of slender reinforced concrete rectangular column confined with CFRP composite. *Composites Part B: Engineering*, *173*, 106939.

[31] Al-Rousan, R. Z., and Issa, M. A. (2018). Stress–strain model and design guidelines for CFRP-confined circular reinforced concrete columns. *Polymer Composites*, *39*(8), 2722-2733.

[32] Issa, M. A., Alrousan, R. Z., and Issa, M. A. (2009). Experimental and parametric study of circular short columns confined with CFRP composites. *Journal of Composites for Construction*, *13*(2), 135-147.

[33] Al-Rousan, R., Nusier, O., Abdalla, K., Alhassan, M., and Lagaros, N. D. (2022). NLFEA of sulfate-damaged circular CFT steel columns confined with CFRP composites and subjected to axial and cyclic lateral loads. *Buildings*, *12*(3), 296.

[34] Khorramian, K., and Sadeghian, P. (2021). Hybrid system of longitudinal CFRP laminates and GFRP wraps for strengthening of existing circular concrete columns. *Engineering Structures*, *235*, 112028.

[35] Iskander, M. G., and Hassan, M. (1998). State of the practice review in FRP composite piling. *Journal of Composites for Construction*, *2*(3), 116-120.

[36] Wang, X., and Wu, Z. (2010). Evaluation of FRP and hybrid FRP cables for super long-span cable-stayed bridges. *Composite Structures*, *92*(10), 2582-2590.

[37] Tarvainen, K., Jolanki, R., Forsman-Grönholm, L., Estlander, T., Pfäffli, P., Juntunen, J., and Kanerva, L. (1993). Exposure, skin protection and occupational skin diseases in the glass-fibre-reinforced plastics industry. *Contact dermatitis*, *29*(3), 119-127.

[38] Tarvainen, K., Jolanki, R., and Estlander, T. (1993). Occupational contact allergy to unsaturated polyester resin cements. *Contact Dermatitis*, *28*(4), 220-224.

[39] Bai, Y. L., Mei, S. J., Li, P., and Xu, J. (2021). Cyclic stress-strain model for large-rupture strain fiber-reinforced polymer (LRS FRP)-confined concrete. *Journal of Building Engineering*, *42*, 102459.

[40] Bai, Y. L., Liu, S. Z., and Mei, S. J. (2024). Compressive behavior and modeling of concrete wrapped by hybrid low-high elongation capacities FRP. *Engineering Structures*, *300*, 117155.

[41] Mei, S. J., Bai, Y. L., Dai, J. G., and Han, Q. (2023). Seismic behaviour of shear critical square RC columns strengthened by large rupture strain FRP. *Engineering Structures*, *280*, 115679.

[42] Fiore, V., Scalici, T., Di Bella, G., and Valenza, A. (2015). A review on basalt fibre and its composites. *Composites Part B: Engineering*, *74*, 74-94.

[43] Sim, J., and Park, C. (2005). Characteristics of basalt fiber as a strengthening material for concrete structures. *Composites Part B: Engineering*, *36*(6-7), 504-512.

[44] Huang, J., Li, T., Zhu, D., Gao, P., and Zhou, A. (2020). Compressive behavior of circular and square concrete column externally confined by different types of basalt fiber–reinforced polymer. *Advances in Structural Engineering*, *23*(8), 1534-1547.

[45] Lopresto, V., Leone, C., and De Iorio, I. (2011). Mechanical characterisation of basalt fibre reinforced plastic. *Composites Part B: Engineering*, *42*(4), 717-723.

DOI: https://doi.org/10.17509/ajse.v6i1.89929
p- ISSN 2776-6098 e- ISSN 2776-5938

[46] Di Ludovico, M., Prota, A., and Manfredi, G. (2010). Structural upgrade using basalt fibers for concrete confinement. *Journal of composites for construction*, *14*(5), 541-552.

[47] Campione, G., La Mendola, L., Monaco, A., Valenza, A., and Fiore, V. (2015). Behavior in compression of concrete cylinders externally wrapped with basalt fibers. *Composites Part B: Engineering*, *69*, 576-586.

[48] Xie, T., and Ozbakkaloglu, T. (2016). Behavior of recycled aggregate concrete-filled basalt and carbon FRP tubes. *Construction and Building Materials*, *105*, 132-143.

[49] Sim, J., and Park, C. (2005). Characteristics of basalt fiber as a strengthening material for concrete structures. *Composites Part B: Engineering*, *36*(6-7), 504-512.

[50] Ma, G., Li, H., and Wang, J. (2013). Experimental study of the seismic behavior of an earthquake-damaged reinforced concrete frame structure retrofitted with basalt fiber-reinforced polymer. *Journal of Composites for Construction*, *17*(6), 04013002.

[51] Sadeghian, P., and Fillmore, B. (2018). Strain distribution of basalt FRP-wrapped concrete cylinders. *Case Studies in Construction Materials*, *9*, e00171.

[52] Pour, A. F., Gholampour, A., & Ozbakkaloglu, T. (2018). Influence of the measurement method on axial strains of FRP-confined concrete under compression. *Composite Structures*, *188*, 415-424.

[53] Vincent, T., and Ozbakkaloglu, T. (2013). Influence of fiber orientation and specimen end condition on axial compressive behavior of FRP-confined concrete. *Construction and Building Materials*, *47*, 814-826.

[54] Shehata, I. A., Carneiro, L. A., and Shehata, L. C. (2002). Strength of short concrete columns confined with CFRP sheets. *Materials and structures*, *35*(1), 50-58.

[55] Pimanmas, A., Hussain, Q., Panyasirikhunawut, A., and Rattanapitikon, W. (2019). Axial strength and deformability of concrete confined with natural fibre-reinforced polymers. *Magazine of Concrete Research*, *71*(2), 55-70.

[56] Saleem, S., Hussain, Q., and Pimanmas, A. (2017). Compressive behavior of PET FRP–confined circular, square, and rectangular concrete columns. *Journal of Composites for Construction*, *21*(3), 04016097.

[57] Yooprasertchai, E., Ejaz, A., Saingam, P., Ng, A. W. M., and Joyklad, P. (2023). Development of stress-strain models for concrete columns externally strengthened with steel clamps. *Construction and Building Materials*, *377*, 131155.

[58] Saingam, P., Ejaz, A., Ali, N., Nawaz, A., Hussain, Q., and Joyklad, P. (2023). Prediction of stress–strain curves for HFRP composite confined brick aggregate concrete under axial load. *Polymers*, *15*(4), 844.

[59] Ghernouti, Y., and Rabehi, B. (2011). FRP-confined short concrete columns under compressive loading: Experimental and modeling investigation. *Journal of Reinforced Plastics and Composites*, *30*(3), 241-255.

[60] Benzaid, R., Mesbah, H., and Chikh, N. E. (2010). FRP-confined concrete cylinders: axial compression experiments and strength model. *Journal of Reinforced Plastics and Composites*, *29*(16), 2469-2488.

[61] Bisby, L. A., Dent, A. J., and Green, M. F. (2005). Comparison of confinement models for FRP wrapped concrete. *ACI Structural Journal*, *102*(1), 62-72.

DOI: https://doi.org/10.17509/ajse.v6i1.89929
p- ISSN 2775-6793 e- ISSN 2775-6815

[62] Wu, H. L., Wang, Y. F., Yu, L., and Li, X. R. (2009). Experimental and computational studies on high-strength concrete circular columns confined by aramid fiber-reinforced polymer sheets. *Journal of Composites for Construction*, *13*(2), 125-134.

[63] Teng, J. G., Huang, Y. L., Lam, L., and Ye, L. P. (2007). Theoretical model for fiber-reinforced polymer-confined concrete. *Journal of Composites for Construction*, *11*(2), 201-210.

[64] Ahmad, S. H., and Shah, S. P. (1982). Complete triaxial stress-strain curves for concrete. *Journal of the Structural Division*, *108*(4), 728-742.

[65] Hussain, Q., Rattanapitikon, W., and Pimanmas, A. (2016). Axial load behavior of circular and square concrete columns confined with sprayed fiber-reinforced polymer composites. *Polymer Composites*, *37*(8), 2557-2567.

[66] Karbhari, V. M., and Gao, Y. (1997). Composite jacketed concrete under uniaxial compression—Verification of simple design equations. *Journal of Materials in Civil Engineering*, *9*(4), 185-193.

[67] Richard, R. M., and Abbott, B. J. (1975). Versatile elastic-plastic stress-strain formula. *Journal of the Engineering Mechanics Division*, *101*(4), 511-515.

DOI: https://doi.org/10.17509/ajse.v6i1.89929
p- ISSN 2776-6098 e- ISSN 2776-5938